The power-law relation between inclusion aspect ratio and porosity: Implications for electrical and elastic modeling

The power-law relation between inclusion aspect ratio and porosity: Implications for electrical and elastic modeling

P. A. Cilli[1,2*], **M. Chapman**[1,2]

[1]Grant Institute, School of GeoSciences, The University of Edinburgh, James Hutton Rd, King's Buildings, Edinburgh, EH9 3FE, UK.

[2]International Centre for Carbonate Reservoirs, Edinburgh, UK.

Key Points:

- The differential effective medium model aspect ratio appears to follow a power-law with porosity
- Introducing a power-law relation leads to improved modeling of 7 public domain data sets
- Introducing a power-law relation leads to alternative models for 5 empirical models

[*]Current address: Department of Earth Sciences, University of Oxford, South Parks Road, Oxford, OX1 3AN, UK

Corresponding author: Phil Cilli, phillip.cilli@earth.ox.ac.uk

Abstract

Geophysicists depend on rock physics relationships to interpret resistivity and seismic velocity in terms of rock porosity, but it has proven difficult to capture the effect of pore geometry on such relations through simple and easy to apply formulae. Inclusion modeling relates moduli to porosity through an equivalent grain or pore aspect ratio but often fails to account for observed trends, whereas empirical relations can be hard to extrapolate beyond their range of validity, often giving incorrect results in the low and high porosity limits. We show that introducing a power-law relationship between porosity and equivalent grain or pore aspect ratio allows inclusion models to reproduce 5 published empirical resistivity-porosity and velocity-porosity relationships, providing a first principles basis for extrapolation to other cases of interest. We find the deviation of resistivity from Archie's law in carbonates is related to a systematic change of grain shape with porosity, and we derive a new relation which fits carbonate resistivity data with similar accuracy to the Humble equation while being correct at high porosity. We then obtain an analog for the Castagna and Pickett relationships for wet, calcitic rocks, which is valid in the low and high porosity limits, giving rise to a new, physically derived V_p/V_s versus porosity model.

1 Introduction

An ongoing challenge in rock physics modeling is understanding how electrical and elastic properties vary with porosity for various rock types. For electrical resistivity, Archie's (Archie, 1942) law is widely believed to produce acceptable results in clean sandstones (Glover, Hole, & Pous, 2000). The electrical properties of carbonates, however, are significantly more complex; a property usually attributed to the diversity of pore types present (Focke & Munn, 1987; Saleh & Castagna, 2004; Salem & Chilingarian, 1999). A modification of Archie's first law, the Humble (Winsauer, Shearin Jr, Masson, & Williams, 1952) equation, may be more accurate in the case of complex pore geometries, but is incorrect in the high-porosity limit. Other models, such as the Shell (Neustaedter, 1968) model, the Borai et al. (1987) model, and the Focke and Munn (1987) relations, are popular in modeling the electrical properties of carbonates, however they are all empirical modifications of Archie's first law, and are not evidently grounded in first-principles physics.

Rock physics models derived from first principles may have the benefit of extrapolating to various rock types, unlike these empirical models which are only applicable

to the rocks where they were calibrated. First principles resistivity models for carbonate rocks, however, are much less developed. In the case of inclusion modeling (Eshelby, 1957), this is due to the difficulty in approximating carbonate grains or pores with spheres and ellipsoids. A notable inclusion model designed specifically for carbonates is that of Xu and Payne (2009).

Just as the electrical properties of carbonates vary with pore types present, the elastic properties of carbonates are also severely dependent on the pore types present. Analogously to the electrical modeling case, significant progress has been made in modeling velocity-porosity trends in the siliciclastic environment (E.g., Dvorkin and Nur (1996); D.-H. Han, Nur, and Morgan (1986); Raymer, Hunt, and Gardner (1980); Vernik and Nur (1992)), however modeling the properties of carbonates, has proven to be more complex (Kittridge, 2014).

Modulus-porosity trends are produced using a range of tools, including empirical, bounding, and inclusions methods. Empirical methods (E.g., Castagna, Batzle, and Kan (1993); D.-H. Han et al. (1986); Pickett (1963)) are useful but challenging to extrapolate beyond their pre-calibrated rock types. Bounding average (E.g., Hill (1952)) and modified bound (E.g., A. Nur, Mavko, Dvorkin, and Galmudi (1998); A. M. Nur, Mavko, Dvorkin, and Gal (1995)) methods can yield comparable accuracy to more sophisticated models (Man & Huang, 2011; Zimmerman, 1991), but can suppress important dependencies on microstructure. As in the electrical modeling case, elastic inclusion models (E.g., Berryman (1980); Kuster and Toksöz (1974); Norris (1985)) are often not preferred since the advantages of having a physics-based approach can be outweighed by the unrealistic assumptions made about the pore geometry. Pride et al. (2017) provide analytical rock physics models which focus on the relationship between effective pressure the electrical and elastic properties of a cracked, porous rock by modeling how porosity changes with pressure, in combination with how moduli change with porosity.

Given that the electrical and elastic properties of rocks are influenced by pore or grain geometry, obtaining realistic carbonate rock physics trends may require characterizing these geometries, which is a prevailing challenge in carbonate rock physics (Anselmetti & Eberli, 1993, 1999; Eberli, Baechle, Anselmetti, & Incze, 2003; Focke & Munn, 1987; Fournier et al., 2018). Some have proposed incorporating pore geometry effects into modeling by using inclusion models with a porosity-dependent pore or grain aspect ra-

tio (Kazatchenko, Markov, & Mousatov, 2004; Kazatchenko, Markov, Mousatov, Pervago, et al., 2006; Markov, Kazatchenko, Mousatov, et al., 2004). An aspect ratio which is piecewise-constant in porosity was proposed by Kazatchenko et al. (2004), while quadratic trends in porosity were considered by Aquino-López, Mousatov, and Markov (2011) and Aquino-López, Mousatov, Markov, and Kazatchenko (2015). More recently, Ellis and Kirstetter (2018) proposed a logarithmic trend between aspect ratio and porosity.

This paper argues for the adoption of a power-law relationship between pore or grain aspect ratio and porosity. We show the power-law relationship, combined with a differential effective medium (DEM) model, fits 7 electrical and elastic data sets with lower misfit than the single aspect ratio DEM model. This power-law model approximates the empirical resistivity-porosity model of Focke and Munn (1987) for carbonates, and has comparable accuracy to the Humble (Winsauer et al., 1952) equation in the range of measured data while being correct at high porosities like Archie's (Archie, 1942) first law. Through this power-law model, we infer that the observed, non-monotonic formation factor-porosity trends in carbonate rocks are the result of an interplay between changing pore shape and proportion of resistive material with porosity. When applying the same power-law relation to carbonate elastic modeling, we obtain a replacement relationship for the empirical $V_p{-}V_s$ relations of Pickett (Pickett, 1963) and Castagna (Castagna et al., 1993) for wet calcitic rocks, which is derived from first principles and correct in both the high and low porosity limit. Finally, a new, first-principles $V_p/V_s{-}\phi$ model for porous rocks also follows from using this power-law relation in the elastic case.

We begin by overviewing the rock physics models used in this paper, before performing inversions on four electrical (Focke & Munn, 1987) data sets for each rock sample's electrical DEM model inclusion aspect ratio. Parameterizing a power-law relation for each data set, we forward model cementation factor and formation factor trends, and compare results with Archie's (Archie, 1942) first law, the Humble (Winsauer et al., 1952) equation, and the empirical trends of Focke and Munn (1987). We do not consider the double layer effect (Waxman & Smits, 1968) in this study, which can be safely neglected in the case of clean carbonates.

We then explore whether there are potential benefits of applying this power-law relation to carbonate elastic modeling. We perform inversion using three elastic data sets (Bakhorji, 2010; Fournier et al., 2011; Verwer, Braaksma, & Kenter, 2008) and param-

eterize the corresponding power-law relation with porosity. We forward model bulk and shear modulus trends for each data set, as well as $Vp{-}Vs$ and $Vp/Vs{-}\phi$ trends, and compare them with the Pickett (Pickett, 1963) and Castagna (Castagna et al., 1993) empirical relations. Throughout this paper, we compare the power-law model's efficiency with the typical, single aspect ratio model using the Corrected Akaike Information Criterion (Hurvich & Tsai, 1989).

2 Modeling Approaches

Rock physics trends are generally studied using collections of samples with at least one varying characteristic, such as porosity. In this paper, we model the relationships between electrical resistivity or elastic moduli and porosity using a number of these collections, each containing laboratory measurements made on many carbonate core samples. We model the data's effective electrical and elastic properties using the differential effective medium (DEM) theory (Berryman, 1992; Mendelson & Cohen, 1982). DEM models are constructed by iteratively adding a small volume of ellipsoidal inclusions into a background material, homogenizing this composite's physical properties, and setting this new homogenized material as the background material for the subsequent iteration until the desired inclusion volume fraction is attained.

2.1 Electrical Modeling Background

Mendelson and Cohen (1982) proposed a DEM model to calculate the overall resistivity of a material consisting of arbitrarily oriented ellipsoidal inclusions in a background of conductive material. By making further assumptions - that the inclusions are perfectly resistive and the background material is initially water - they derived Archie's (Archie, 1942) first law:

$$F = \phi^{-m}\,; \tag{1}$$

where ϕ is the rock's pore volume fraction or porosity, and m is the rock's cementation factor. The rock's formation factor, F, can be defined as $F = \sigma_w/\sigma$ in a fully saturated rock, where σ_w is the saturating water's conductivity and σ is the effective conductivity. As electrical conductivity and resistivity are mutually reciprocal, F can be viewed as the bulk resistivity of a fluid-flooded rock normalized by the resistivity of the flood-

ing fluid. We note equation 1 is missing the coefficient a presented in the more general Humble (Winsauer et al., 1952) equation (e.g., Glover (2016)):

$$F = a\phi^{-m}\,. \tag{2}$$

Salem and Chilingarian (1999) showed by analysis of well log data that m is strongly dependent on the shape of rock grains and pores. This dependence of m on pore geometry has been investigated throughout the literature (Glover, 2010; Glover et al., 2000; Mendelson & Cohen, 1982; Nigmatullin, Dissado, & Soutougin, 1992). Further to this, Focke and Munn (1987) showed cementation factor can be non-constant across a range of porosities in carbonates. The derivation of Archie's first law by Mendelson and Cohen (1982) showed cementation factor m is a function of grain aspect ratio through depolarization factors L_p, where $p \in \{1, 2, 3\}$ refers to the grain's semi-major axes. Depolarization factors relate a background electrical potential field in a homogeneous material to the perturbation potential field caused by the presence of an uncharged, conducting ellipsoidal grain. Following Mendelson and Cohen (1982), this paper is written with the convention $\sum L_p = 1$.

The expression for cementation factor m derived by Mendelson and Cohen (1982) is:

$$m = \frac{1}{3}\sum_{p=1}^{3}\left\langle (1 - L_p)^{-1}\right\rangle\,; \tag{3}$$

where angled brackets $\langle\cdot\rangle$ denote the average over the distribution of grain aspect ratios present. Mendelson and Cohen (1982) made the simplification $L_1 = L$ and $L_2 = L_3 = (1 - L)/2$ in equation 3 and averaged over all inclusion orientations for a single grain aspect ratio to produce:

$$m = \frac{5 - 3L}{3(1 - L^2)}\,; \tag{4}$$

as was also derived by Gelius and Wang (2008) and T. Han, Clennell, Josh, and Pervukhina (2015). Fournier et al. (2011, 2014, 2018) refer to the elastic inclusion aspect ratio, α, as the "equivalent pore aspect ratio", or "EPAR", which we adopt in this

paper. In line with this convention, we abbreviate the electrical DEM model aspect ratio parameter to "equivalent grain aspect ratio", or "EGAR".

2.2 Elastic Modeling Background

The elastic DEM model can be described by the coupled differential equations (Berryman, 1992):

$$(1-\phi)\frac{d}{d\phi}\left[K^*(\phi)\right] = \left(K_2 - K^*(\phi)\right)P^{(*2)}; \tag{5}$$

$$(1-\phi)\frac{d}{d\phi}\left[\mu^*(\phi)\right] = \left(\mu_2 - \mu^*(\phi)\right)Q^{(*2)}; \tag{6}$$

with the initial conditions $K^*(0) = K_1$ and $\mu^*(0) = \mu_1$. Subscript 1 refers to background properties, while subscript 2 refers to inclusion properties. Thus, in the case of ellipsoidal pores embedded in a mineral background, K_1 and μ_1 are the mineral bulk and shear moduli; K_2 and μ_2 are the pore fluid bulk and shear moduli; K^* and μ^* are the porous rock's effective bulk and shear moduli; and ϕ is the porosity.

Functions P and Q (Berryman, 1980) are geometrical functions which are combinations of select elements of the T tensor, first put forward by Wu (1966). The T tensor relates the strain field in a solitary ellipsoidal inclusion to the strain field applied at the boundary of the material in which the inclusion sits. As is the T tensor, functions P and Q are dependent on the ellipsoidal inclusion's aspect ratio α, as well as the elastic moduli and Poisson's ratios of the inclusion and background materials. It is evident from equations 5 and 6 that the inclusion aspect ratio term α is present in this formulation of the elastic DEM model solely through functions P and Q. The superscript $(*2)$ in equations 5 and 6 indicate P and Q are to be calculated assuming the background material in which the inclusion is embedded is in fact the effective medium material itself.

3 Description of Data

We investigate seven public-domain laboratory data sets which come from carbonate outcrop, surface borehole, and well cores in various global localities. The data have varied porosity ranges, diverse pore network architectures, and are approximately monomineralic. Three of these laboratory data sets have elastic measurements and four have electrical measurements.

We use the carbonate data of Focke and Munn (1987) for our electrical modeling tests, as described in Appendix A. We refer to this data as the "FM" data for brevity. We use the measurements made on limestones with intergranular porosity; dolostones with intergranular porosity; sucrosic dolostones with intercrystalline porosity; and oolitic limestones and dolostones with moldic porosity. Sucrosic dolostones are recrystallized dolostones with a coarse texture (Dunham, 1962), while moldic pores are fabric-selective pores formed by the dissolution of grains (e.g., Choquette and Pray (1970)).

Following Focke and Munn (1987), we treat the first three rock types as a single data set due to their petrophysical similarities, and model the moldic carbonates as three separate data sets, partitioned by their permeabilities: $0 \leq k < 0.1$ mD; $0.1 \leq k < 1$ mD; and $1 \leq k < 100$ mD. We chose to perform our electrical modeling tests on intergranular and sucrosic carbonate samples as the pore structure associated with these rocks can often be reasonably approximated by an inclusion model. In contrast to this, we also chose to perform our electrical model testing on carbonates with moldic porosity as the assumptions of inclusion models can be highly inappropriate when applied to these rocks, which can lead to poor modeling outcomes.

We model three of the four public domain elastic data sets investigated by Kittridge (2014). These carbonate laboratory data sets are from Verwer et al. (2008), Bakhorji (2010), and Fournier et al. (2011), which we will refer to as the "Verwer", "Bakhorji", and "Fournier" data sets for brevity. Appendix A and Kittridge (2014) present further details on these data sets. For elastic modeling, we use only dry measurements made on the subset of cores comprised of approximately 100% calcite in the Bakhorji and Fournier data sets, and 100% dolomite in the Verwer data set. This experimental design allows us to perform all elastic modeling assuming a two-phase rock, composed of a single-mineral matrix and air-filled pore space. In doing this, we minimize modeling uncertainties due to errors in matrix and fluid compositions.

4 Electrical Modeling

To investigate the relationship between EGAR and porosity in electrical DEM modeling, we inverted for the EGAR of each core sample individually by minimizing the difference in the measured and modeled formation factor using equations 1 and 4, assuming oblate spheroidal inclusions.

We displayed the inverted EGARs against measured sample porosity ϕ on a log-log scale, as shown in Figure 1. The central observation underpinning our modeling is the observed linear trend. We placed a line of best fit through each data set's inverted EGARs, with the form:

$$\log \alpha = C + \xi \log \phi \,, \tag{7}$$

where C and ξ are the constant and gradient of the line of best fit respectively.

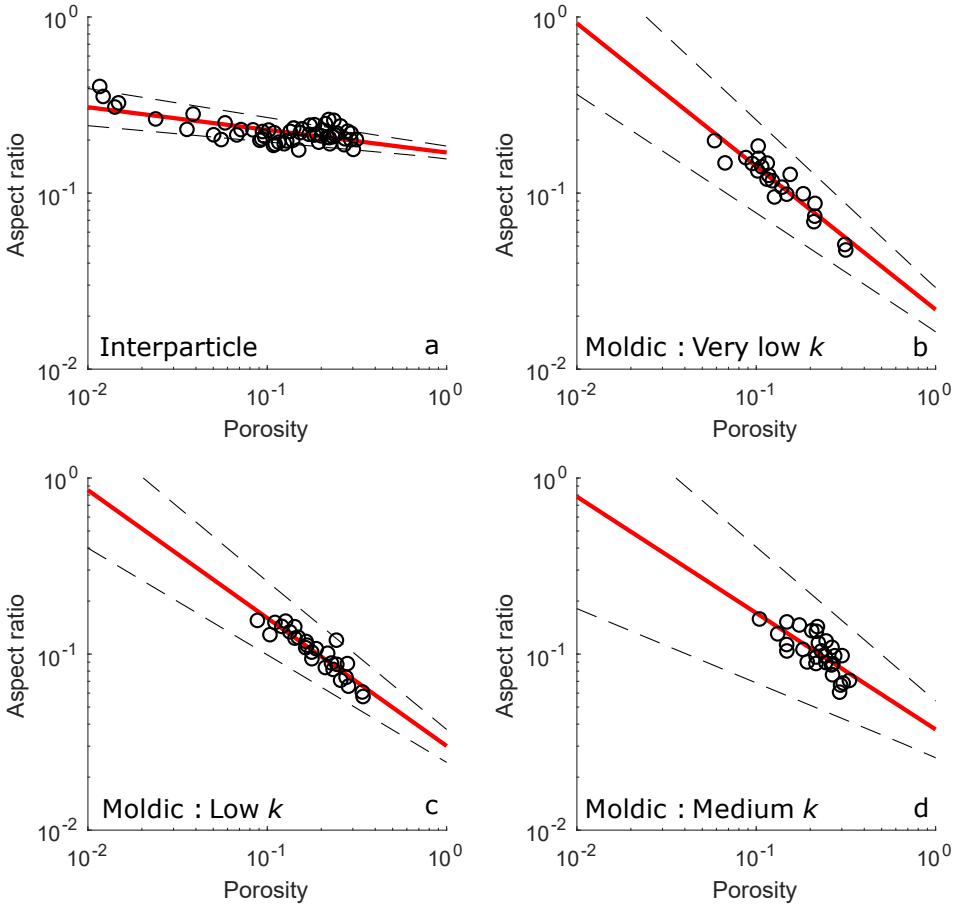

Figure 1. Inverted EGARs from the FM data using the electrical DEM model of Mendelson and Cohen (1982). Lines of best fit and their 95% confidence intervals are shown. Subfigures show a) Interparticle porosity; b) Moldic porosity with $0 \leq k < 0.1$ mD; c) Moldic porosity with $0.1 \leq k < 1$ mD; and d) Moldic porosity with $1 \leq k < 100$ mD.

Figure 1 also shows each linear fit's 95% confidence interval on C and ξ for each data set, calculated from the linear regressions' covariance matrices.

It follows from equation 7 that a best-fitting intercept C and gradient ξ become parameters $\{\Gamma, \xi\}$ in the power-law:

$$\alpha = \Gamma \phi^{\xi} \,. \tag{8}$$

As the inverted EGARs in Figure 1 are not independent of ϕ, we used the solution parameters $\{\Gamma_0, \xi_0\}$ which were obtained from the line of best fit for each data set as the starting point in a non-linear inversion to find the true solution parameters $\{\Gamma^*, \xi^*\}$. To find parameters $\{\Gamma^*, \xi^*\}$ for each data set, we inverted the nested equations 1, 4, and 8, 100 times using a fast simulated annealing algorithm (Szu & Hartley, 1987). We then chose the optimal solution for each data set to be that which had the lowest l_1-norm misfit between the logarithm of the data set's measured and modeled formation factors. We chose this misfit metric for electrical inversion to reduce preferential model fitting at low porosities. Initial and final solutions, $\{\Gamma_0, \xi_0\}$ and $\{\Gamma^*, \xi^*\}$, are found in Table 1 for all data sets, where we see only small updates in solution parameters between the two inversions.

Substituting equation 8 into equations 4 and 1, assuming rock grains are oblate spheroids, we obtain a new, explicit expression for formation factor:

$$F = \phi^{\left[3\left[\frac{\Gamma^2\phi^{2\xi}\left(\sqrt{\frac{\phi^{-2\xi}}{\Gamma^2}-1}-\arcsin\left[\Gamma\phi^{\xi}\sqrt{\frac{\phi^{-2\xi}}{\Gamma^2}-1}\right]\right)^2}{\left(\Gamma^2\phi^{2\xi}-1\right)^3}+1\right]-\frac{5-\frac{3\phi^{-2\xi}\left(1-\frac{\arcsin\left[\Gamma\phi^{\xi}\sqrt{\frac{\phi^{-2\xi}}{\Gamma^2}-1}\right]}{\sqrt{\frac{\phi^{-2\xi}}{\Gamma^2}-1}}\right)}{\Gamma^2\left(\frac{\phi^{-2\xi}}{\Gamma^2}-1\right)}}{3}\right]} \,. \tag{9}$$

We forward-modeled cementation factor and formation factor trends for all electrical data sets using parameters $\{\Gamma^*, \xi^*\}$ and equation 9, as shown in Figures 2 and 3 respectively. The set of green curves display the power-law model, which fits both the formation and cementation factor data more accurately than the best fitting Archie's law, shown in dashed red. They also approximate the empirical models of Focke and Munn (1987), displayed with dotted black lines. The Humble equation may provide a suitable fit to the data in Figure 3, however it is incorrect in the limit when $\phi \to 1$. As $\xi < 0$

for all four modeled data sets, and as grains are assumed to be oblate spheroids, the power-law model is only valid on porosities above that where $\alpha = 1$. When $\alpha = 1$, $m = 3/2$ and the power-law model reduces to the model of Sen, Scala, and Cohen (1981), indicated by an empty black square in Figure 2.

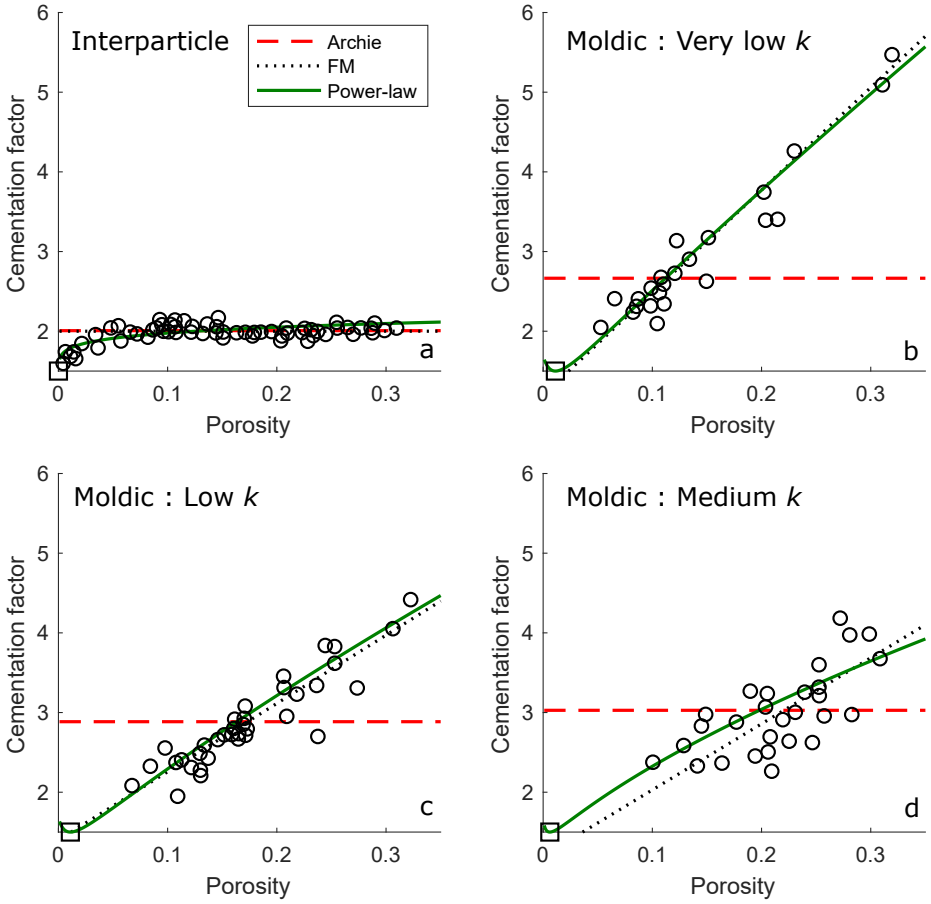

Figure 2. Forward-modeled cementation factor for the FM data using the power-law DEM model (solid), Archie's first law (dashed), and Focke and Munn's empirical relationships (dotted). The lower bound of the power-law model's valid porosity range is also shown (square). Subfigures show a) Interparticle porosity; b) Moldic porosity with $0 \leq k < 0.1$ mD; c) Moldic porosity with $0.1 \leq k < 1$ mD; and d) Moldic porosity with $1 \leq k < 100$ mD.

Table 1 summarizes the electrical inversion results, with a 50% to 85% improvement in the residual sum of squares (RSS) error on Archie's law across all FM data sets. To quantitatively establish the preferred model for each data set, we use the Corrected Akaike Information Criterion (Hurvich & Tsai, 1989), as reviewed in Appendix B. All

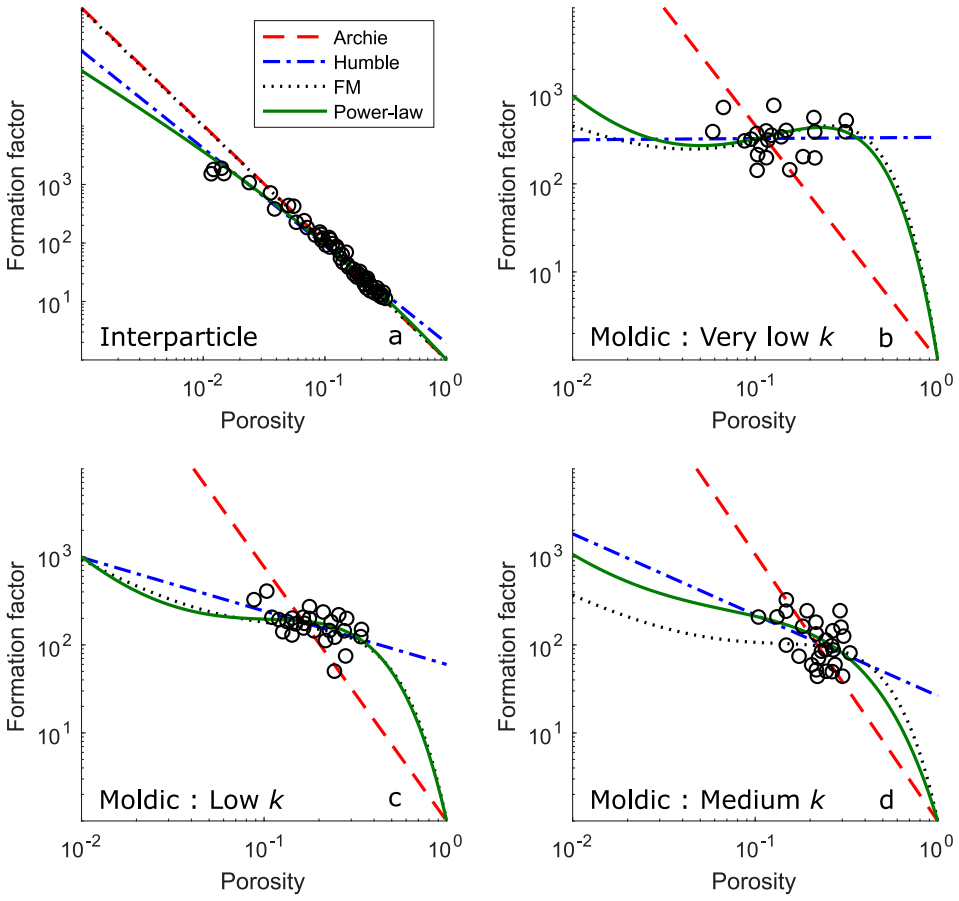

Figure 3. Forward-modeled formation factor for the FM data using the power-law DEM model (solid), Archie's first law (dashed), the Humble equation (dot-dashed), and Focke and Munn's empirical relationships (dotted). Subfigures show a) Interparticle porosity; b) Moldic porosity with $0 \leq k < 0.1$ mD; c) Moldic porosity with $0.1 \leq k < 1$ mD; and d) Moldic porosity with $1 \leq k < 100$ mD.

modeling log-relative likelihoods were much greater than 10, meaning there is compelling evidence supporting the use of the power-law model over Archie's law on all electrical data sets.

There is a theoretical possibility for certain model parameters that aspect ratio can be greater than unity, which would be inconsistent with the modeling assumption of oblate spheroids. As such, we show the range of porosities where the power-law model is valid in Table 1.

The points of inflexion and turning points in the power-law forward-modeled formation factor trends are not present in Archie's law but are key features in the empirical models of Focke and Munn (1987). We infer these special points are due to the competing effects of inclusion geometry and pore volume fraction on a porous rock's overall resistivity. A porous rock's resistivity decreases with increasing porosity due to a reduction in the amount of insulating material. The resistivity of a rock comprised of ellipsoidal grains, however, increases with grain eccentricity, as shown by Mendelson and Cohen (1982). These two effects compete in the FM data, where inclusions become more eccentric with increasing porosity, leading to the non-monotonic formation factor trends observed by Focke and Munn (1987) and in Figure 3.

5 Elastic Modeling

We have seen how including a power-law between equivalent grain aspect ratio and porosity in an electrical DEM model can lead to effective modeling of rocks with complex pore geometries. Given this result, we now examine if a power-law between pore aspect ratio and porosity in an elastic DEM model is beneficial for the elastic modeling of rocks with complex pore geometries.

5.1 Bulk Modulus Modeling

To investigate the relationship between bulk modulus EPAR and porosity in elastic DEM modeling, we first calculated a measured effective bulk and shear modulus for each core of the three elastic data sets using the laboratory-measured P- and S-wave velocities, and bulk density. With known mineralogy and porosity from experimental data, and mineral moduli shown in Table 2, we inverted for each sample's bulk modulus EPAR by minimizing the difference between measured and modeled bulk modulus using equa-

Table 1. Electrical modeling results.

Electrical inversion (Pore type)	n	$\{\Gamma_0, \xi_0\}$	$\{\Gamma^*, \xi^*\}$	m^*_{Archie}	a^*_{Humble}	m^*_{Humble}	Valid porosities	% RSS decrease on Archie's Law	Log-relative likelihood ΔAIC_C
Focke and Munn (1987) (Interparticle)	55	{0.170, -0.129}	{0.173, -0.122}	2.01	1.97	1.67	$\phi > 10^{-6}$	68.8	61.8
Focke and Munn (1987) (Moldic: Very low k)	22	{0.022, -0.813}	{0.018, -0.895}	2.67	338	-0.01	$\phi > 0.011$	85.6	40.0
Focke and Munn (1987) (Moldic: Low k)	27	{0.030, -0.727}	{0.026, -0.808}	2.89	59.8	0.61	$\phi > 0.011$	83.5	46.1
Focke and Munn (1987) (Moldic: Medium k)	28	{0.037, -0.661}	{0.036, -0.650}	3.03	26.3	0.92	$\phi > 0.006$	52.5	18.3

tions 5 and 6. As was done in the electrical case (Section 4), we then calculated initial model parameters $\{\Gamma_0, \xi_0\}$ for each data set by fitting a line of best fit through the cross-plot of inverted EPARs and measured porosities on a log-log scale. Following this, we inverted equations 5, 6, and 8 for $\{\Gamma^*, \xi^*\}$ 100 times using a fast simulated annealing algorithm, choosing the final solution parameters as those which led to the lowest misfit out of all 100 solutions, as was done in the electrical modeling case. Unlike the inversion for electrical model parameters, the minimized objective function in the inversion for bulk modulus $\{\Gamma^*, \xi^*\}$ was the l_2-distance between the measured and modeled bulk moduli for each data set.

Figure 4 shows the inverted bulk modulus EPARs for each sample, as well as the line of best fit used to calculate $\{\Gamma_0, \xi_0\}$ for each elastic data set, and the 95% confidence intervals associated with these fits. Parameters $\{\Gamma_0, \xi_0\}$ and $\{\Gamma^*, \xi^*\}$ are found in Table 3 for all elastic data sets, where we see only small updates in solution parameters between the two inversions.

We forward-modeled best-fitting $\phi - K$ trends using equations 5, 6, and 8 given the optimal parameters $\{\Gamma^*, \xi^*\}$. We also calculated the best fitting EPAR which is constant in porosity, α^*_{DEM}, for each data set and forward-modeled the corresponding Single-α DEM $\phi - K$ trends for comparison (Figure 5). Figures 5a and 5b show the power-law DEM model appears more accurate than Single-α DEM, particularly at low porosities. In fact, the percentage decrease in elastic modeling RSS error by using the power-law DEM model over Single-α DEM model is seen in Table 3 to be over 60% in the Bakhorji data. Figure 5c is an example of the power-law model collapsing to a Single-α DEM model, with $\xi^* \approx 0$, and hence $\Gamma^* \approx \alpha^*_{DEM}$ (Table 3).

Table 3 shows the log-relative likelihood (ΔAIC_C) for all bulk modulus elastic modeling comparisons, which is greater than ten for the Bakhorji and Fournier data sets. Following the model selection convention described in Appendix B, we conclude there is compelling evidence for the use of the power-law model in these cases. In modeling the Verwer data, when the power-law model approximates the special case of a Single-α DEM model, both models generate a similar $\phi - K$ trend (Figure 5c) but the Single-α DEM model has fewer parameters. The corresponding ΔAIC_C is -1.9, which supports the use of the Single-α model. We also show the range of porosities where the model is valid in Table 3, noting this is effectively all porosities on all elastic data sets.

Table 2. Elastic parameters used in modeling.

Constituent	Bulk Modulus (Pa)	Shear Modulus (Pa)	Density (kg/m^3)	References
Calcite	76.8×10^9	32.0×10^9	2.71×10^3	Simmons (1965)
Dolomite	94.9×10^9	45.0×10^9	2.87×10^3	Humbert and Plicque (1972)
Quartz	36.6×10^9	45.0×10^9	-	T. Han, Best, MacGregor, Sothcott, and Minshull (2011) Mavko, Mukerji, and Dvorkin (2009)
Clay	20.9×10^9	6.85×10^9	-	Mavko et al. (2009); Tosaya (1982); T. Han et al. (2011)
Water	2.3×10^9	0	-	T. Han et al. (2011)
Air	1.01×10^5	0	1.29	Mavko et al. (2009)

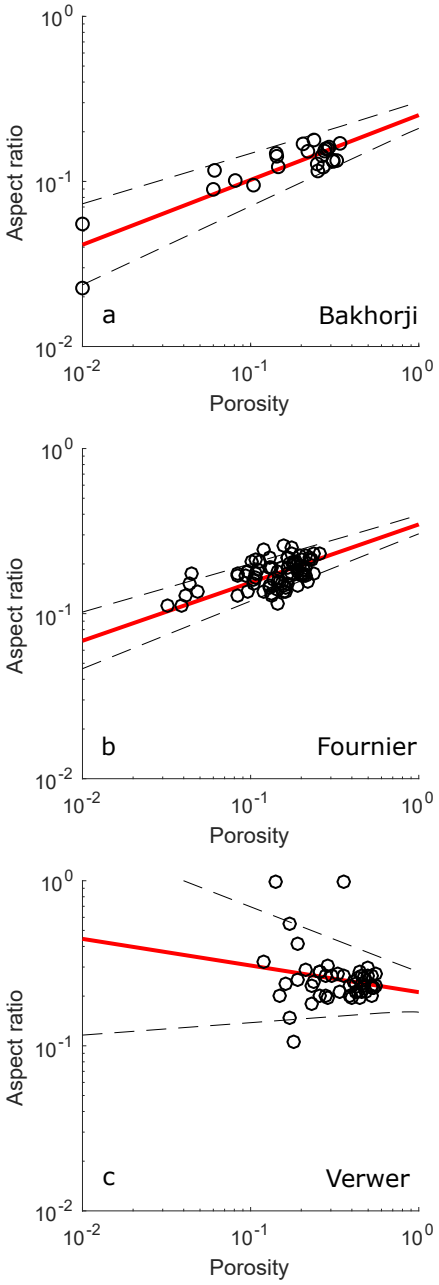

Figure 4. Inverted EPARs (circles) from bulk modulus data. Lines of best fit (solid red) and their 95% confidence intervals (dashed black) are shown. Subfigures show a) the Bakhorji data set; b) the Fournier data set; and c) the Verwer data set.

Table 3. Elastic modeling results.

Elastic inversion	n	$\{\Gamma_0, \xi_0\}$	$\{\Gamma^*, \xi^*\}$	α^*_{DEM}	Valid porosities	% RSS decrease on Single-α DEM	Log-relative likelihood ΔAIC_C
Bakhorji (2010) K-Inversion	24	{0.252, 0.393}	{0.257, 0.387}	0.13	All ϕ	60.5	19.7
Bakhorji (2010) μ-Inversion	24	{0.273, 0.561}	{0.257, 0.521}	0.12	All ϕ	48.8	13.6
Fournier et al. (2011) K-Inversion	80	{0.347, 0.352}	{0.277, 0.238}	0.17	All ϕ	22.1	17.9
Fournier et al. (2011) μ-Inversion	80	{0.379, 0.562}	{0.296, 0.439}	0.13	All ϕ	41.6	40.8
Verwer et al. (2008) K-Inversion	51	{0.211, -0.116}	{0.231, -0.046}	0.25	$\phi > 10^{-13}$	0.7	-1.9
Verwer et al. (2008) μ-Inversion	51	{0.185, 0.024}	{0.204, 0.140}	0.17	All ϕ	4.3	0.0
Combined calcites K-Inversion	104	{0.312, 0.345}	{0.264, 0.246}	0.17	All ϕ	17.0	17.3
Combined calcites μ-inversion	104	{0.338, 0.542}	{0.249, 0.381}	0.13	All ϕ	26.3	29.6

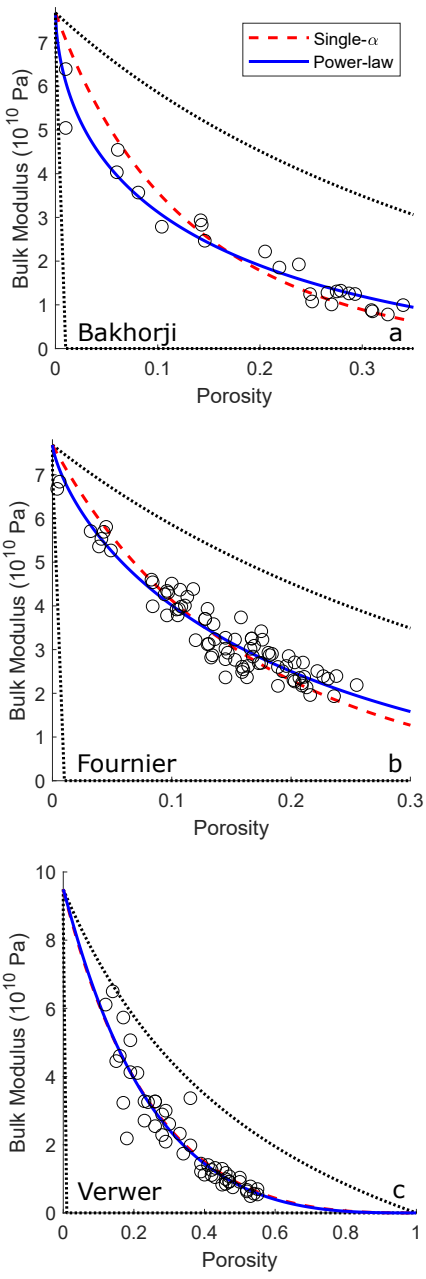

Figure 5. Forward-modeled bulk modulus from the power-law DEM (solid blue) and optimal Single-α DEM (dashed red) models, as well as measured data (circles), and the Hashin-Shtrikman bounds (dotted black bounding curves). Subfigures show a) the Bakhorji data set; b) the Fournier data set; and c) the Verwer data set. Notice the power-law and Single-α DEM trends are almost identical in the Verwer data.

5.2 Shear Modulus and V_p-V_s Modeling

A shortcoming of elastic inclusion modeling is the practical inability to model both a rock's bulk and shear modulus using the same EPAR. This is observed by Fournier et al. (2011, 2014, 2018), and is usually attributed to the presence of asperities in pores. In fact, Fournier et al. (2014, 2018) investigate the relationship between bulk and shear modulus EPARs and exploit this relationship to effectively characterize different lithologies. In this section, we first mathematically relate the bulk and shear modulus EPARs of a rock before deriving V_p-V_s and V_p/V_s-ϕ models based on elastic DEM theory and the proposed power-law relationship.

We denote the rock's porosity-dependent bulk and shear modulus EPARs by $\alpha_K(\phi)$ and $\alpha_\mu(\phi)$ respectively. Similarly, $\{\Gamma_K, \xi_K\}$ and $\{\Gamma_\mu, \xi_\mu\}$ are their respective power-law model parameters.

We inverted for the shear modulus parameters $\{\Gamma_\mu, \xi_\mu\}$ of the three elastic data sets by the same method as bulk modulus inversion but minimizing shear modulus misfit. Figure 6 shows the parameterized linear $\phi - \alpha$ trends on a log-log plot after shear modulus inversion.

Initial and final shear modulus parameters are displayed in Table 3 and are distinguished by the subscript "0" and superscript "*" respectively.

Figure 7 shows that forward-modeling $\phi - \mu$ trends seems to generate more accurate fits over standard, Single-α DEM methods, in the Bakhorji and Fournier data sets. Comparing the proposed power-law model and the best-fitting Single-α DEM model in terms of log-relative likelihoods, there is compelling evidence that the power-law model is the best model for use on the Bakhorji and Fournier shear modulus data, with $\Delta AIC_C > 10$ (Table 3). It is approximately equally likely the power-law and Single-α DEM models are the best model by the AIC_C metric for the Verwer data set as $\Delta AIC_C = 0.0$.

From equation 8, the ratio of $\alpha_K(\phi)$ and $\alpha_\mu(\phi)$ is:

$$\alpha_\mu(\phi) = \frac{\Gamma_\mu}{\Gamma_K}\phi^{\bar{\xi}}\alpha_K(\phi)\ ; \tag{10}$$

where $\bar{\xi} = \xi_\mu - \xi_K$.

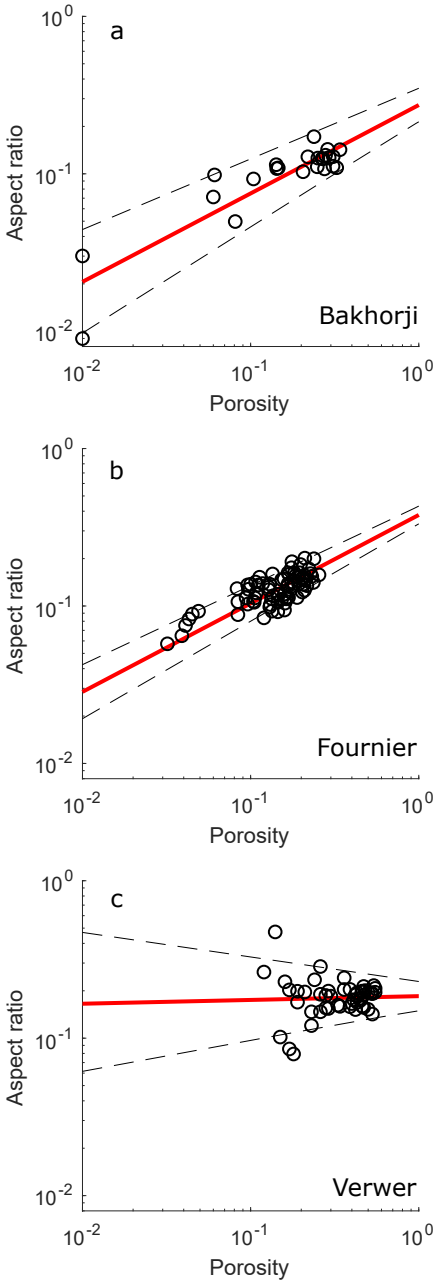

Figure 6. Inverted EPARs (circles) from shear modulus data. Lines of best fit (solid red) and their 95% confidence intervals (dashed black) are shown. Subfigures show a) the Bakhorji data set; b) the Fournier data set; and c) the Verwer data set.

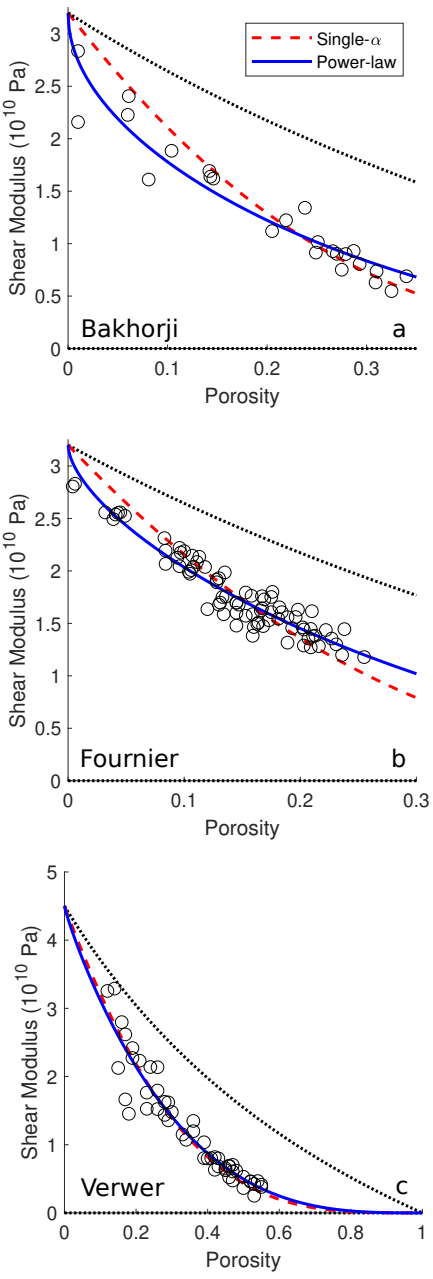

Figure 7. Forward-modeled shear modulus from the power-law DEM (solid blue) and optimal Single-α DEM (dashed red) models, as well as measured data (circles), and the Hashin-Shtrikman bounds (dotted black bounding curves). Subfigures show a) the Bakhorji data set; b) the Fournier data set; and c) the Verwer data set. Notice the power-law and Single-α DEM trends are almost identical in the Verwer data.

In Table 3, we observe Γ^*_μ and Γ^*_K are similar for the Bakhorji and Fournier data sets, implying α_K and α_μ are similar in the high porosity limit. Given the observed similarity of Γ^*_μ and Γ^*_K in the Fournier and Bakhorji data sets, we modeled a calcite V_p/V_s-ϕ relationship using the approximation:

$$\alpha_\mu(\phi) \approx \phi^{\bar{\xi}} \alpha_K(\phi) \ . \tag{11}$$

Thus we see parameter $\bar{\xi}$ quantifies the difference in how bulk and shear modulus EPARs change with porosity.

Figure 8 shows the inverted bulk and shear modulus EPARs for each calcitic core sample, taken from the Bakhorji and Fournier data sets, and the forward-modeled α_μ-α_K trend for calcites. We forward-modeled effective bulk and shear modulus trends using the elastic DEM model (equations 5 and 6) and equation 11. Following this, we forward-modeled a V_p-V_s trend for dry calcitic rocks using densities from Table 2. Water-saturating the modeled dry V_p-V_s trend using Gassmann (1951) fluid substitution, we compare the model's behavior with the empirical relations of Pickett (1963) and Castagna et al. (1993) in Figure 8 for wet calcite. The power-law DEM model evidently approximates the empirical models in the range of the data, while having the added benefits of being correct in the high and low porosity limits and being based on first principles.

Figure 8 also shows the forward-modeled V_p/V_s-ϕ trend calculated for dry calcite using the V_p and V_s trends obtained through equation 11. The laboratory measured data are shown and generally agree with this analytically derived V_p/V_s-ϕ trend.

6 Discussion

We have presented a modified DEM model which fits 7 public-domain electrical and elastic data sets more accurately than the typical DEM modeling approach. This improved fitting, however, is at the expense of an extra model parameter, which we have justified using log-relative likelihood analysis. Model parameters ξ and Γ both have a physical interpretation. Parameter ξ signifies the rate at which EPAR or EGAR changes with porosity. It follows that ξ may be an indicator of how a rock is affected by the physical processes which alter pore geometry such as diagenesis. Parameter Γ indicates the

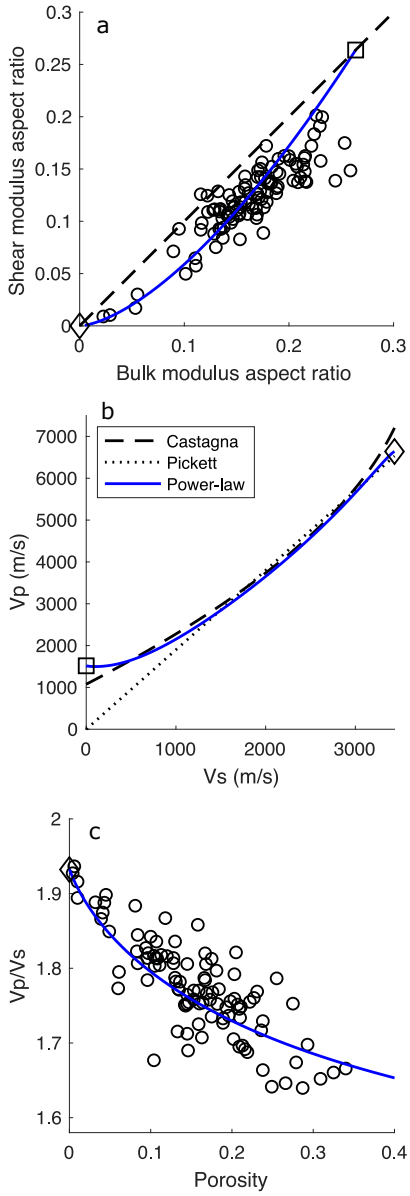

Figure 8. V_p-V_s modeling of the combined Bakhorji and Fournier calcitic data sets. Diamond markers denote 100% calcite, while squares denote 100% fluid. a) The α_μ-α_K trend (solid blue) and inverted EPARs from dry laboratory measurements (circles) are shown with a dashed 1:1 line for reference. b) The Gassmann-wetted power-law DEM V_p-V_s trend (solid blue) is shown with the Castagna et al. (1993) (dashed black) and Pickett (1963) (dotted black) empirical relations for wet calcite. c) The dry power-law DEM V_p/V_s-ϕ trend (solid blue) is shown with dry laboratory measurements (circles).

limiting EPAR or EGAR when $\phi \rightarrow 1$, and therefore indicates the expected stiffness of a rock at high porosities.

We have selected data with highly-constrained mineralogy and fluid content to minimize errors in EPAR or EGAR inversion. The fluid content and hence its electrical resistivity is largely unknown in the experiments of Focke and Munn (1987). However, Focke and Munn (1987) note that formation factor does not appear to be affected by the brine's resistivity in clean carbonates. The extension of the work in this paper to multimineralic and multifluid rocks may have larger modeling errors as additional, mixing models must also be used. The proposed power-law electrical model is not designed to account for the double-layer effect (Waxman & Smits, 1968) as all solid phases are assumed to be insulating.

Archie's (Archie, 1942) contribution was to show that resistivity of fully saturated sandstones followed a simple law given by equation 1, but unfortunately it became clear that carbonates showed more complex relationships. Several authors tried to address this variability by allowing cementation factor to vary with porosity in Archie's law, deducing values that varied from 1 to greater than 4 (Focke & Munn, 1987; Verwer, Eberli, & Weger, 2011). Although undeniably useful, these porosity varying forms can be read as definitions of cementation factor; any combination of formation factor and porosity can be modeled with a suitable choice of the value m. Our goal in this paper was to link this implicit cementation factor-porosity relationship directly to details of the pore-structure, leading the way to making the formulation predictive.

The presented power-law model has the same number of model parameters as the critical porosity model of Mukerji, Berryman, Mavko, and Berge (1995). This power-law model can act as an approximate critical porosity model when $\xi < 0$, as well as the Single-α DEM model when $\xi = 0$. The power-law model's form when $\xi > 0$ cannot be approximated by the typical critical porosity model, however, which may make the power-law model preferable in the case of an unknown critical porosity.

The sign of parameter ξ^* is positive in the elastic case, and negative in the electrical case. This is due to the elastic model being constructed with inclusions of fluid being embedded into a background of matrix, while the electrical model is constructed with inclusions of grain material being embedded into a background of fluid.

A major drawback of modeling with the Humble equation is that it is non-physical in the high-porosity limit. The proposed electrical power-law DEM model addresses this issue. It models carbonate data with comparable accuracy to the Humble equation (Figure 3) and uses the same number of model parameters, but is correct when $\phi \to 1$, like Archie's first law.

Our claim of a non-constant relationship between porosity and EPAR may seem to contrast with that of Fournier et al. (2018), who conclude EPAR is constant in mineralogy and porosity for carbonates with a given dominant pore type. Fournier et al. (2018), however, do observe a change in EPAR with porosity for a given carbonate facies (e.g., in spherulites from offshore Brazil). Further, Fournier et al. (2018) show diagenetic alteration in carbonates, such as vug-forming dissolution, leads to altered EPARs. Our findings may therefore be consistent with the foundational works of Fournier et al. (2011, 2014, 2018) if our investigated samples are diagenetically altered or differ in dominant pore type across different porosities.

7 Conclusion

We argue that introducing a power-law relationship between porosity and aspect ratio improves the efficiency of modeling the variation of electrical properties with porosity, and also observe benefits when using this power-law relation in elastic modeling. Much interpretation of resistivity or velocity in terms of porosity depends on a small number of empirical relationships, which are known to break down in many important cases. Our power-law leads to alternative relationships which are derived from first principles, reproduce the empirical relations over much of the porosity range, and are exactly correct in the high and low porosity limits. This provides a basis for extrapolating the empirical relationship to different geological conditions, as well as an alternative in situations where the empirical models are known to fail, as is the case with Archie's first law in many carbonates. Use of the power-law model to link electrical and elastic properties would require a data set with both measurements, but we hope the proposed models are a step towards multiphysics modeling from first principles.

A Data review

The resistivity data of Focke and Munn (1987) are laboratory resistivity measurements made on reservoirs core from offshore Qatar. No pore fluid conductivity or salin-

ity measurements were provided in the original publication of Focke and Munn (1987). Rather, it was noted that the experimental pore fluid simulated formation water for all data sets. Similarly, mineralogical measurements were not available, but it was noted that most plugs were made of clean carbonates. Having no tabulated data, we digitized the data manually.

We studied only subsets of the Verwer (Verwer et al., 2008), Fournier (Fournier et al., 2011), and Bakhorji (Bakhorji, 2010) elastic data sets to minimize the influence of confounding factors on our modeling results. Table A.1, adapted from Kittridge (2014), shows data set details. We selected only dry measurements for elastic modeling made on approximately monomineralic samples.

We studied the 51-sample subset from the Verwer data set which contained porosity, dry V_p, dry V_s, dry bulk density measurements, and had 100% dolomite composition to the nearest integer by XRD analysis. We modeled this data assuming 100% dolomite mineralogy using the elastic parameters shown in Table 3. We used the dry core measurements of the Bakhorji data set at 20 MPa confining pressure from the loading stage of the loading-then-unloading experimental regime, as was done by Kittridge (2014). We studied the 24-sample subset from this Saudi-D reservoir data which contained at least 90% calcite by volume. The median composition of these samples was 99% calcite, so we modeled the data set using a 100% calcite mineralogy with the elastic parameters shown in Table 3. We studied the dry, elastic measurements of the Fournier data set made at 20 MPa confining pressure on all 80 calcitic cores and modeled this data set with a 100% calcite mineralogy.

B Corrected Akaike Information Criterion

The Akaike Information Criterion (AIC) (Akaike, 1973) is a model selection criterion based in Information theory which estimates the most likely amount of information lost when approximating measured data generated by a true, unknown model, with a candidate, fitted model. The AIC does this by estimating the fitted model's expected Kullback-Leibler divergence (Kullback & Leibler, 1951) from the true, unknown model which generates the measured data. Hurvich and Tsai (1989) formulate the AIC as:

$$AIC = n\left(\log \hat{s}^2 + 1\right) + 2\left(p + 1\right) ; \tag{B.1}$$

Table A.1. Summary of elastic core data sets analyzed (Adapted from Kittridge (2014)).

Source	Location	Type	#Spl	Lab velocity	Description	Additional descriptor(s)
Verwer *et al.* (2008)	Cap Blanc of the Llucmajor Platform, Mallorca	Outcrop and surface borehole (3)	250	Wet (deaired brine 3% NaCl) and dry; Peff 10 MPa; Ppore 0.1 MPa; 1 MHz	Miocene; low- and high-Mg calcite, dolomite, aragonite. Mostly dolomitic	XRD, petrography, texture (granular, crystalline)
Bakhorji (2010)	Arab-D reservoir (Saudi Arabia) with seven wells	Wells	37	Wet and dry; Pconf 5-25 MPa (increasing, decreasing stress); ∼1 MHz	Limestone or Dolomite (<1% noncarbonate)	Samples characterized as macro, micro, dual porosity. Petrography, SEM, mercury porosimetry
Fournier *et al.* (2011)	Four outcrop locations South East France	Outcrop	80	Dry; Pconf 2.5, 5, 10, 20, and 40 MPa; Ppore 0.1 MPa; 1 MHz	Lower Cretaceous platform; microporous limestone	All grainstone texture, absence of intergranular, intercrystalline, or moldic porosity

where n is the number of samples, p is the number of model parameters, and $\hat{s}$ is the maximum likelihood estimate of the measured data's variance.

The AIC is biased in the case of small n, where it tends to favor models with larger p (Hurvich & Tsai, 1989). As our data sets are relatively small, we compare models using the Corrected Akaike Information Criterion (AIC_C) (Hurvich & Tsai, 1989), which is more accurate in small n. Hurvich and Tsai (1989) derive the AIC_C as:

$$AIC_C = AIC + \frac{2\,(p+1)\,(p+2)}{n-p-2}\,. \tag{B.2}$$

We see the second, additive term on the right-hand side of equation B.2 goes to 0 when $n \gg p$, approximating the AIC, and is non-negligible when p and n are comparable. The difference, ΔAIC_C, in the AIC_C values of a reference and candidate model indicates the evidence for using one model over the other. It is the logarithm of the relative likelihood of the two models, conditional on the model parameters and residuals from the data (Burnham & Anderson, 2002). We thus refer to the ΔAIC_C as the *log-relative likelihood* throughout this paper.

For example, we can compare the two-parameter, power-law (superscript "PL") model with the best single-parameter (superscript "DEM") model using the ΔAIC_C, which we define as:

$$\Delta AIC_C = AIC_C^{\mathrm{DEM}} - AIC_C^{\mathrm{PL}}\,. \tag{B.3}$$

The value of ΔAIC_C here indicates the evidence that the proposed power-law model is more likely to be more efficient than the single-aspect ratio ("Single-α") DEM model. Burnham and Anderson (2002, 2004) provide useful rules of thumb for the interpreting the log-relative likelihood of competing models, analogous to the popular advice of Raftery (1996) or Jeffreys (1998) in the Bayesian model selection literature. Applied specifically to our formulation of ΔAIC_C, these guidelines suggest if $\Delta AIC_C > 0$, the power-law model is considered to be the best model, however if:

1. $0 < \Delta AIC_C < 2$: Single-α DEM has substantial evidence as best model.
2. $4 < \Delta AIC_C < 7$: Single-α DEM has considerably less evidence.
3. $\Delta AIC_C > 10$: Single-α DEM has essentially no evidence.

We reframe these guidelines to focus on the power-law model, proposing and discussing results in terms of the complimentary case:

4. $\Delta AIC_C > 10$: Power-law model has compelling evidence as best model.

When $\Delta AIC_C < 0$, Single-α DEM is accepted as the best model and the magnitude of the log-relative likelihood is used to measure the evidence that the power-law model is the best model under Burnham and Anderson's guidelines.

Acknowledgments

The authors would like to thank Petrobras and Shell for their sponsorship of the International Center for Carbonate Reservoirs (ICCR), and for permission to publish this work from the VSP project. We thank Andrew Curtis, Ian Main, Rachel Wood, and Giorgos Papageorgiou at the University of Edinburgh, Tongcheng Han at the China University of Petroleum, Qingdao, and Angus Best at the UK National Oceanograpy Center, Southampton, for their support in this work. The data on which this paper is based can be obtained in Focke and Munn (1987), Verwer et al. (2008), Bakhorji (2010), and Fournier et al. (2011).

References

Akaike, H. (1973). Information theory and an extension of the maximum likelihood principle. In B. N. Petrov & F. Csaki (Eds.), *Proceedings of the 2nd international symposium on information theory* (Vol. 4, pp. 267–281).

Anselmetti, F. S., & Eberli, G. P. (1993). Controls on sonic velocity in carbonates. *Pure and Applied geophysics*, *141*(2-4), 287–323.

Anselmetti, F. S., & Eberli, G. P. (1999). The velocity-deviation log: A tool to predict pore type and permeability trends in carbonate drill holes from sonic and porosity or density logs. *AAPG bulletin*, *83*(3), 450–466.

Aquino-López, A., Mousatov, A., & Markov, M. (2011). Model of sand formations for joint simulation of elastic moduli and electrical conductivity. *Journal of Geophysics and Engineering*, *8*(4), 568.

Aquino-López, A., Mousatov, A., Markov, M., & Kazatchenko, E. (2015). Modeling and inversion of elastic wave velocities and electrical conductivity in clastic formations with structural and dispersed shales. *Journal of Applied Geophysics*, *116*, 28–42.

519 Archie, G. E. (1942). The electrical resistivity log as an aid in determining some
520 reservoir characteristics. *Transactions of the AIME*, *146*(1), 54–62.
521 Bakhorji, A. M. (2010). *Laboratory measurements of static and dynamic elastic*
522 *properties in carbonate* (Unpublished doctoral dissertation). University of Al-
523 berta.
524 Berryman, J. G. (1980). Long-wavelength propagation in composite elastic media II.
525 Ellipsoidal inclusions. *The Journal of the Acoustical Society of America*, *68*(6),
526 1820–1831.
527 Berryman, J. G. (1992). Single-scattering approximations for coefficients in Biot's
528 equations of poroelasticity. *The Journal of the Acoustical Society of America*,
529 *91*(2), 551–571.
530 Borai, A., et al. (1987). A new correlation for the cementation factor in low-porosity
531 carbonates. *SPE Formation Evaluation*, *2*(04), 495–499.
532 Burnham, K. P., & Anderson, D. R. (2002). *Multimodel inference: A practical*
533 *information-theoretical approach* (2nd ed.). Colorado Cooperative Fish and
534 Wildlife Research Unit, Colorado State University, Fort Collins, CO 80523-
535 1484, USA: Springer-Verlag New York.
536 Burnham, K. P., & Anderson, D. R. (2004). Multimodel inference: Understand-
537 ing aic and bic in model selection. *Sociological methods & research*, *33*(2), 261–
538 304.
539 Castagna, J. P., Batzle, M. L., & Kan, T. K. (1993). Rock physics - The link be-
540 tween rock properties and avo response. In J. P. Castagna & M. M. Backus
541 (Eds.), *Offset-dependent reflectivity - Theory and practice of AVO analysis:*
542 *Investigations in Geophysics.* Society of Exploration Geophysicists.
543 Choquette, P. W., & Pray, L. C. (1970). Geologic nomenclature and classification of
544 porosity in sedimentary carbonates. *American Association of Petroleum Geolo-*
545 *gists Bulletin*, *54*(2), 207–250.
546 Dunham, R. J. (1962). Classification of carbonate rocks according to depositional
547 texture. In *Classification of carbonate rocks - a symposium* (pp. 108–121).
548 U.S.: American Association of Petroleum Geologist.
549 Dvorkin, J., & Nur, A. (1996). Elasticity of high-porosity sandstones: Theory for
550 two North Sea data sets. *Geophysics*, *61*(5), 1363–1370.
551 Eberli, G. P., Baechle, G. T., Anselmetti, F. S., & Incze, M. L. (2003). Factors con-

552 trolling elastic properties in carbonate sediments and rocks. *The Leading Edge*,
553 *22*(7), 654–660.
554 Ellis, M., & Kirstetter, O. (2018). Resistivity anisotropic inclusion model for clastic
555 sediments. In *Seg technical program expanded abstracts 2018* (pp. 3488–3492).
556 Society of Exploration Geophysicists.
557 Eshelby, J. D. (1957). The determination of the elastic field of an ellipsoidal inclu-
558 sion, and related problems. *Proc. R. Soc. Lond. A*, *241*(1226), 376–396.
559 Focke, J. W., & Munn, D. (1987). Cementation exponents in Middle Eastern car-
560 bonate reservoirs. *SPE Formation Evaluation*, *2*(2), 155–167.
561 Fournier, F., Léonide, P., Biscarrat, K., Gallois, A., Borgomano, J., & Foubert, A.
562 (2011). Elastic properties of microporous cemented grainstones. *Geophysics*,
563 *76*(6), E211–E226.
564 Fournier, F., Léonide, P., Kleipool, L., Toullec, R., Reijmer, J. J. G., Borgomano,
565 J., ... Van Der Molen, J. (2014). Pore space evolution and elastic properties
566 of platform carbonates (Urgonian limestone, Barremian-Aptian, SE France).
567 *Sedimentary Geology*, *308*, 1–17.
568 Fournier, F., Pellerin, M., Villeneuve, Q., Teillet, T., Hong, F., Poli, E., ...
569 Hairabian, A. (2018). The equivalent pore aspect ratio as a tool for pore
570 type prediction in carbonate reservoirs. *AAPG Bulletin*, *102*(7), 1343.
571 Gassmann, F. (1951). Verteljahrsschrift der naturforschenden gesellschaft in Zurich.
572 *Uber die elastizitat poroser medien*, *96*, 1–23.
573 Gelius, L.-J., & Wang, Z. (2008). Modelling production caused changes in conductiv-
574 ity for a siliciclastic reservoir: A differential effective medium approach. *Geo-*
575 *physical Prospecting*, *56*(5), 677–691.
576 Glover, P. W. J. (2010). A generalized Archie's law for n phases. *Geophysics*, *75*(6),
577 E247–E265.
578 Glover, P. W. J. (2016). Archie's law - A reappraisal. *Solid Earth*, *7*(4), 1157.
579 Glover, P. W. J., Hole, M. J., & Pous, J. (2000). A modified Archie's law for two
580 conducting phases. *Earth and Planetary Science Letters*, *180*(3-4), 369–383.
581 Han, D.-H., Nur, A., & Morgan, D. (1986). Effects of porosity and clay content on
582 wave velocities in sandstones. *Geophysics*, *51*(11), 2093–2107.
583 Han, T., Best, A. I., MacGregor, L. M., Sothcott, J., & Minshull, T. A. (2011). Joint
584 elastic-electrical effective medium models of reservoir sandstones. *Geophysical*

Prospecting, *59*(4), 777–786.

Han, T., Clennell, M. B., Josh, M., & Pervukhina, M. (2015). Determination of effective grain geometry for electrical modeling of sedimentary rocks. *Geophysics*, *80*(4), D319–D327.

Hill, R. (1952). The elastic behaviour of a crystalline aggregate. *Proceedings of the Physical Society. Section A*, *65*(5), 349.

Humbert, P., & Plicque, F. (1972). Propriétés élastiques des carbonates rhombohédriques monocristallins: Calcite, magnésite et dolomie. *Comptes Rendus de l'Académie des Sciences de Paris*, *275*, 391–394.

Hurvich, C. M., & Tsai, C.-L. (1989). Regression and time series model selection in small samples. *Biometrika*, *76*(2), 297–307.

Jeffreys, H. (1998). *The theory of probability*. OUP Oxford.

Kazatchenko, E., Markov, M., & Mousatov, A. (2004). Joint inversion of acoustic and resistivity data for carbonate microstructure evaluation. *Petrophysics*, *45*(02).

Kazatchenko, E., Markov, M., Mousatov, A., Pervago, E., et al. (2006). Simulation of the electrical resistivity of dual-porosity carbonate formations saturated with fluid mixtures. *Petrophysics*, *47*(01).

Kittridge, M. G. (2014). Investigating the influence of mineralogy and pore shape on the velocity of carbonate rocks: Insights from extant global data sets. *Interpretation*, *3*(1), SA15–SA31.

Kullback, S., & Leibler, R. A. (1951). On information and sufficiency. *The annals of mathematical statistics*, *22*(1), 79–86.

Kuster, G. T., & Toksöz, M. N. (1974). Velocity and attenuation of seismic waves in two-phase media: Part I. Theoretical formulations. *Geophysics*, *39*(5), 587–606.

Man, C.-S., & Huang, M. (2011). A simple explicit formula for the Voigt-Reuss-Hill average of elastic polycrystals with arbitrary crystal and texture symmetries. *Journal of Elasticity*, *105*(1-2), 29–48.

Markov, M., Kazatchenko, E., Mousatov, A., et al. (2004). Prediction of the acoustic velocities, electrical and thermal conductivities of carbonate formations applying self-consistent methods. In *SPWLA 45th annual logging symposium.*

Mavko, G., Mukerji, T., & Dvorkin, J. (2009). *The rock physics handbook: Tools for*

seismic analysis of porous media. Cambridge University Press.

Mendelson, K. S., & Cohen, M. H. (1982). The effect of grain anisotropy on the electrical properties of sedimentary rocks. *Geophysics*, *47*(2), 257–263.

Mukerji, T., Berryman, J., Mavko, G., & Berge, P. (1995). Differential effective medium modeling of rock elastic moduli with critical porosity constraints. *Geophysical Research Letters*, *22*(5), 555–558.

Neustaedter, R. H. (1968). Log evaluation of deep ellenburger gas zones. In *Spe deep drilling and development symposium.*

Nigmatullin, R., Dissado, L., & Soutougin, N. (1992). A fractal pore model for Archie's law in sedimentary rocks. *Journal of Physics D: Applied Physics*, *25*(1), 32.

Norris, A. N. (1985). A differential scheme for the effective moduli of composites. *Mechanics of materials*, *4*(1), 1–16.

Nur, A., Mavko, G., Dvorkin, J., & Galmudi, D. (1998). Critical porosity: A key to relating physical properties to porosity in rocks. *The Leading Edge*, *17*(3), 357–362.

Nur, A. M., Mavko, G., Dvorkin, J., & Gal, D. (1995). Critical porosity: The key to relating physical properties to porosity in rocks. In *SEG technical program expanded abstracts 1995* (pp. 878–881). Society of Exploration Geophysicists.

Pickett, G. R. (1963). Acoustic character logs and their applications in formation evaluation. *Journal of Petroleum technology*, *15*(06), 659–667.

Pride, S. R., Berryman, J. G., Commer, M., Nakagawa, S., Newman, G. A., & Vasco, D. W. (2017). Changes in geophysical properties caused by fluid injection into porous rocks: analytical models. *Geophysical Prospecting*, *65*(3), 766–790.

Raftery, A. E. (1996). Approximate Bayes factors and accounting for model uncertainty in generalised linear models. *Biometrika*, *83*(2), 251–266.

Raymer, L. L., Hunt, E. R., & Gardner, J. S. (1980). An improved sonic transit time-to-porosity transform. In *SPWLA 21st annual logging symposium.*

Saleh, A. A., & Castagna, J. P. (2004). Revisiting the Wyllie time average equation in the case of near-spherical pores. *Geophysics*, *69*(1), 45–55.

Salem, H. S., & Chilingarian, G. V. (1999). The cementation factor of Archie's equation for shaly sandstone reservoirs. *Journal of Petroleum Science and En-*

gineering, *23*(2), 83–93.

Sen, P. N., Scala, C., & Cohen, M. H. (1981). A self-similar model for sedimentary rocks with application to the dielectric constant of fused glass beads. *Geophysics*, *46*(5), 781–795.

Simmons, G. (1965). *Single crystal elastic constants and calculated aggregate properties* (Tech. Rep.). Dallas, Texas: Southern Methodist University.

Szu, H., & Hartley, R. (1987). Fast simulated annealing. *Physics letters A*, *122*(3-4), 157–162.

Tosaya, C. (1982). *Acoustical properties of clay-bearing rocks* (Unpublished doctoral dissertation). Stanford University.

Vernik, L., & Nur, A. (1992). Ultrasonic velocity and anisotropy of hydrocarbon source rocks. *Geophysics*, *57*(5), 727–735.

Verwer, K., Braaksma, H., & Kenter, J. A. (2008). Acoustic properties of carbonates: Effects of rock texture and implications for fluid substitution. *Geophysics*, *73*(2), B51–B65.

Verwer, K., Eberli, G. P., & Weger, R. (2011). Effect of pore structure on electrical resistivity in carbonates. *AAPG bulletin*, *95*(2), 175–190.

Waxman, M. H., & Smits, L. J. M. (1968). Electrical conductivities in oil-bearing shaly sands. *Society of Petroleum Engineers Journal*, *8*(02), 107–122.

Winsauer, W. O., Shearin Jr, H., Masson, P., & Williams, M. (1952). Resistivity of brine-saturated sands in relation to pore geometry. *AAPG bulletin*, *36*(2), 253–277.

Wu, T. T. (1966). The effect of inclusion shape on the elastic moduli of a two-phase material. *International Journal of Solids and Structures*, *2*(1), 1–8.

Xu, S., & Payne, M. A. (2009). Modeling elastic properties in carbonate rocks. *The Leading Edge*, *28*(1), 66–74.

Zimmerman, R. W. (1991). *Compressibility of sandstones* (Vol. 29). Elsevier.